

Leaking from the phase space of the Riemann-Liouville fractional standard map

J. A. Méndez-Bermúdez

*Instituto de Física, Benemérita Universidad Autónoma de Puebla, Apartado Postal J-48,
Puebla 72570, Mexico*

Kevin Peralta-Martinez

*Instituto de Física, Benemérita Universidad Autónoma de Puebla, Apartado Postal J-48,
Puebla 72570, Mexico*

José M. Sigarreta

*Facultad de Matemáticas, Universidad Autónoma de Guerrero, Carlos E. Adame No.54
Col. Garita, Acalpulco Gro. 39650, Mexico*

Edson D. Leonel

*Universidade Estadual Paulista (UNESP) - Departamento de Física, Av. 24A, 1515 –
Bela Vista – CEP: 13506-900 – Rio Claro – SP – Brazil*

Abstract

In this work we characterize the escape of orbits from the phase space of the Riemann-Liouville (RL) fractional standard map (fSM). The RL-fSM, given in action-angle variables, is derived from the equation of motion of the kicked rotor when the second order derivative is substituted by a RL derivative of fractional order α . Thus, the RL-fSM is parameterized by K and $\alpha \in (1, 2]$ which control the strength of nonlinearity and the fractional order of the RL derivative, respectively. Indeed, for $\alpha = 2$ and given initial conditions, the RL-fSM reproduces Chirikov's standard map. By computing the survival probability $P_S(n)$ and the frequency of escape $P_E(n)$, for a hole of height h placed in the action axis, we observe two scenarios: When the phase space is ergodic, both scattering functions are scale invariant with the typical escape time $n_{\text{typ}} = \exp\langle \ln n \rangle \propto (h/K)^2$. In contrast, when the phase space is not ergodic, the scattering functions show a clear non-universal and parameter-dependent behavior.

1. Introduction

When discussing about the generic transition to chaos, in the context of the Kolmogorov–Arnold–Moser (KAM) theorem, probably one of the most popular example models is the kicked rotor (KR); see e.g. [1]. The KR, which represents a free rotating stick in an inhomogeneous field that is periodically switched on in instantaneous pulses, is described by the second order differential equation

$$\ddot{x} + K \sin(x) \sum_{n=0}^{\infty} \delta\left(\frac{t}{T} - n\right) = 0. \quad (1)$$

Here, $x \in [0, 2\pi]$ is the angular position of the stick, K is the kicking strength, T is the kicking period (that we set to one from now on), and δ is Dirac’s delta function. A very useful approach to the dynamics of the KR is by studying its stroboscopic projection, which is well known as Chirikov’s standard map (CSM) [1, 2, 3]:

$$\begin{aligned} p_{n+1} &= p_n - K \sin(x_n), \\ x_{n+1} &= x_n + p_{n+1}, \quad \text{mod } (2\pi), \end{aligned} \quad (2)$$

where p corresponds to the angular momentum of the KR’s stick. Indeed, CSM is known to represent the local dynamics of several Hamiltonian systems and is by itself a paradigm model of the KAM scenario.

In order to account for dynamical features not present in KAM’s scenario, modified versions of CSM have been introduced. Among them we can highlight the dissipative version of CSM (also known as Zaslavsky map) [4] and the discontinuous version of CSM [5]. Moreover, by substituting the second-order derivative in the equation of the KR by the Riemann-Liouville (RL) derivative ${}_0D_t^\alpha$, the RL fractional KR is obtained [6]:

$${}_0D_t^\alpha x + K \sin(x) \sum_{n=0}^{\infty} \delta(t - n) = 0, \quad 1 < \alpha \leq 2. \quad (3)$$

Above

$$\begin{aligned} {}_0D_t^\alpha x(t) &= D_t^m {}_0I_t^{m-\alpha} x(t) \\ &= \frac{1}{\Gamma(m-\alpha)} \frac{d^m}{dt^m} \int_0^t \frac{x^\tau d\tau}{(t-\tau)^{\alpha-m+1}}, \quad m-1 < \alpha \leq m, \end{aligned}$$

with $D_t^m = d^m/dt^m$ and ${}_0I_t^m f(t)$ is a fractional integral given by

$${}_0I_t^m f(t) = \frac{1}{\Gamma(m)} \int_0^t (t - \tau)^{m-1} f(\tau) d\tau.$$

Notice that now $p(t) \equiv {}_0D_t^{\alpha-1} x(t)$.

Correspondingly, the stroboscopic projection of the RL fractional KR is known as the RL fractional standard map (RL-fSM) which reads as [6]

$$\begin{aligned} p_{n+1} &= p_n - K \sin(x_n), \\ x_{n+1} &= \frac{1}{\Gamma(\alpha)} \sum_{i=0}^n p_{i+1} V_\alpha(n - i + 1) \\ &\quad + \frac{b}{\Gamma(\alpha - 1)} (n + 1)^{\alpha-2}, \quad \text{mod } (2\pi). \end{aligned} \quad (4)$$

Here, Γ is the Gamma function and

$$V_\alpha(m) = m^{\alpha-1} - (m - 1)^{\alpha-1}.$$

Note that the sum in the equation for the position in map (4) makes the RL-fSM to have memory, meaning that the future $(n + 1)$ -state depends on the entire orbit and not on the present n -state only. The property of memory is known to be present in maps derived from fractional differential equations [7], such as the RL-fSM of Eq. (4), but also in maps derived from fractional integral equations [8] and in maps derived from fractional integro-differential equations [9].

It is important to add that for $b = 0$, in the case $\alpha = 2$, the RL-fSM reproduces CSM. Therefore in this work we consider the RL-fSM in the form

$$\begin{aligned} p_{n+1} &= p_n - K \sin(x_n), \\ x_{n+1} &= \frac{1}{\Gamma(\alpha)} \sum_{i=0}^n p_{i+1} V_\alpha(n - i + 1), \quad \text{mod } (2\pi), \end{aligned} \quad (5)$$

where $1 < \alpha \leq 2$ is assumed. The RL-fSM has no periodicity in p and cannot be considered on a torus like CSM.

In contrast with CSM, depending on the strength of nonlinearity K and the fractional order of the RL derivative α , the RL-fSM generates attractors (fixed points, stable periodic trajectories, slow converging and slow diverging trajectories, ballistic trajectories, and fractal-like structures) and/or chaotic

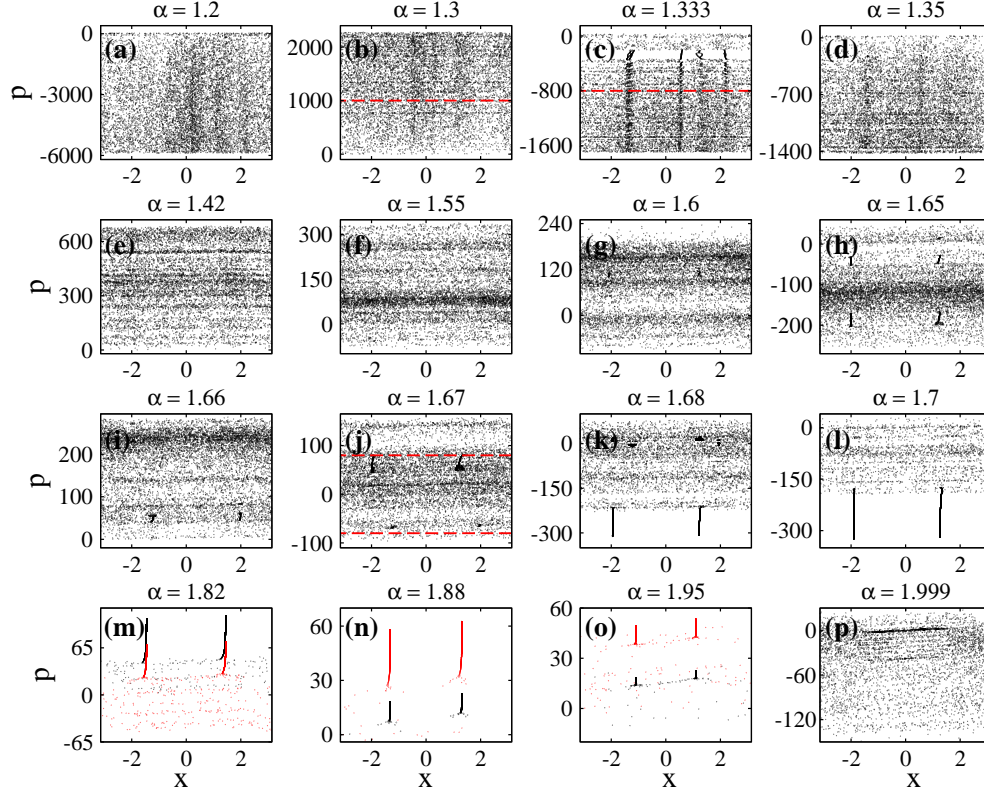


Figure 1: Poincaré surfaces of section for the Riemann-Liouville fractional standard map of Eq. (5) with $K = 4.6$ and several values of α . A single initial condition with $x_0 = 0$ and a random $p_0 \in (0, 2\pi/100)$ was iterated 10^4 times (black dots). Red dots in panels (m,n,o) represent the orbit of a second initial condition. Red dashed lines in (b,c,j) indicate the position of holes in the action axis at $h = 1000, 800$ and 80 , respectively.

trajectories [6]. Moreover, trajectories may intersect and attractors may overlap [10]. As an example, in Fig. 1 we present Poincaré surfaces of section for the RL-fSM with $K = 4.6$ and several values of α . In this figure we can observe the convergence to stable periodic trajectories (see the period-two periodic orbits in panels (k) to (o)), the existence of unstable periodic trajectories (see the period-four periodic orbit in panel (c)), the overlap of trajectories (see e.g. the red and black period-two periodic orbits in panel (m)), as well as quite uniform chaotic trajectories (see panels (a) and (d)). Similar Poincaré surfaces of section are observed for other values of K . Thus, we can safely state that the RL-fSM is a richer dynamical system as compared to CSM.

Since its introduction by Edelman and Tarasov [6], several studies on the RL-fSM have been reported and other fractional versions of the standard map have also been introduced, see e. g. [12, 13, 10, 7, 11, 14, 15, 16, 17]. Among those studies we highlight that: Already in Refs. [12, 13] the dissipative fSM (which is the fractional version of Zaslavsky map [4]) was introduced; the Caputo fSM (i.e. the fSM derived from the KR with a Caputo fractional derivative) was introduced and contrasted with the RL-fSM in Ref. [10]; the α -family of the fSM, where the order of the fractional derivative is not restricted to $1 < \alpha \leq 2$, was defined in Refs. [11, 15].

Coming back to the RL-fSM, even though many of its properties have been already studied, as far as we know, its scattering properties have not been explored yet. Thus, in this work we undertake this task and characterize the escape of orbits from the phase space of the RL-fSM. Specifically, in this work we compute the survival probability $P_S(n)$ and the frequency of escape $P_E(n)$ for a hole of height h placed in the action axis. Then, we analyze both scattering quantities as a function of K and α , the parameters of the RL-fSM.

2. Scattering setup and scattering measures

Scattering experiments are used to probe the properties of target systems by measuring transport or scattering quantities [18]. In classical scattering we can cite two main scattering setups: in one setup particles are measured after scattered by a target system while in another setup the target system is characterized by means of particle leaking. Here we use the second setup where the leak can be a physical hole (such as an opening in the boundary of a billiard table) or a subset of the phase space (i.e., a threshold in one or more variables). In either case an orbit, with initial conditions inside the dynamical system, that reaches the hole is considered to escape from the system, see e.g. [19, 20, 21]. Two well-known quantities used in studies of classical leaking are the survival probability $P_S(n)$ and the frequency of escape $P_E(n)$; so we compute both here.

We open the RL-fSM by placing a hole on a subset of the phase space of constant action. Moreover, since the phase space of (5) is symmetric (i.e. $\langle p_n \rangle = 0$) we define the hole as two horizontal lines at $p = \pm h$ in the Poincaré surfaces of section. As examples, in Figs. 1(b), 1(c) and 1(j) we show (as red dashed lines) holes with $h = 1000, 800$ and 80 , respectively. Therefore, we analyze the escape of trajectories from map (5) as a function of the parameters K , α and h , controlling the nonlinearity of the map, the

fractional order of the RL derivative and the openness of the scattering setup, respectively.

For each combination of (K, h, α) , we consider an ensemble of 10^5 orbits having as initial conditions $x_0 = 0$ and random p_0 uniformly distributed in the interval $(0, 2\pi/100)$. Each initial condition is evolved in time according to map (5). If, along the orbit, the action surpasses the hole, i.e. $|p_n| > h$, we determine that the orbit has escaped from the RLfSM and a new initial condition is selected. We count the number of trajectories $N_S(n)$, that at time n , have not escaped yet from the RL-fSM, then we compute $P_S(n)$ as $P_S(n) = N_S(n)/M$. Simultaneously, by counting the total number of orbits that have escaped up to time n , we construct the histogram for the frequency of escape $P_E(n)$.

3. Survival probability and frequency of escape

Since the RL-fSM displays a rich and diverse dynamics we characterize the orbits leaking from its phase space first when the phase space is ergodic and later when it is not. Also, without loss of generality in the following numerical calculations we consider two relatively large values of K (6.908745 and 7.5) which allowed us to get good statistics in reasonable computer times. We note that some aspects of the dynamics of the RL-fSM with $K = 6.908745$ have been explored in [6], so we decided to use this value of K in our study. Moreover, we verified that our conclusions do not depend on these values of K .

3.1. Ergodic phase space

In Figs. 2(a,b) we present the survival probability $P_S(n)$ as a function of n for the RL-fSM with $K = 6.908745$ and several combinations of α and h . The values of α we choose in Figs. 2(a,b) produce an ergodic phase space, see Fig. A.1; or at least we did not observe the formation of structures in phase space for the values of h we consider. Note that we are considering here the value of $\alpha = 2$, see the magenta curves in Fig. 2(b), which corresponds to CSM whose scattering properties have already been studied in [20, 21]. From Figs. 2(a,b) we note that $P_S(n)$ shows an almost perfect exponential decay of the form

$$P_S(n) = \exp\left(-\frac{n}{\mu}\right), \quad (6)$$

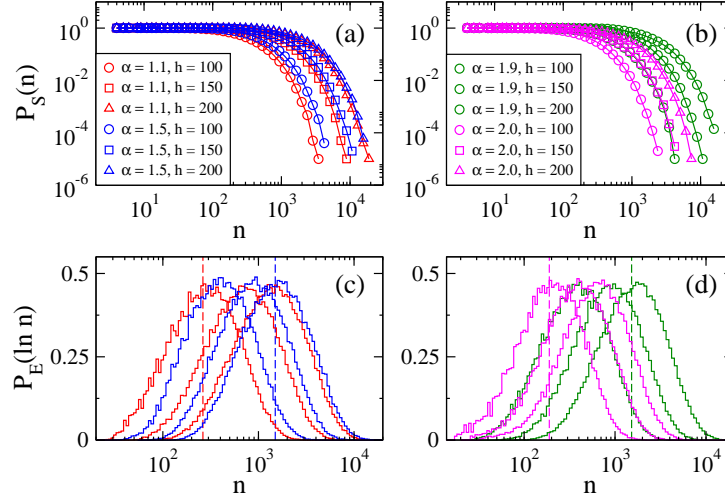


Figure 2: (a,b) Survival probability $P_S(n)$ as a function of n (symbols) for the RL-fSM with $K = 6.908745$ and several combinations of α and h ($\alpha = 1.1$ in red, $\alpha = 1.5$ in blue, $\alpha = 1.9$ in green, and $\alpha = 2$ in magenta; h grows from left to right, as labeled in the figure). Full lines are fittings of the data with Eq. (6). Each curve was constructed by the use of $M = 10^5$ orbits. (c,d) Histograms for the frequency of escape $P_E(\ln n)$. Same color code as in (a,b). Vertical dashed lines are the typical escape times $n_{\text{typ}} = \exp\langle \ln n \rangle$ (they are shown for four histograms only to avoid figure saturation). Each histogram was constructed by the use of $M = 10^5$ orbits.

which is typical of strongly chaotic systems [18, 22] (see also [20, 21]). Indeed, the full lines in Figs. 2(a,b) are fittings of Eq. (6) to the data (symbols), where μ has been used as fitting parameter.

Concerning the frequency of escape $P_E(n)$, we observed that it increases as a function of n until it reaches a maximum at a given iteration number, then it decreases and approaches zero asymptotically for $n \rightarrow \infty$. However, since to observe the complete increase and decrease of $P_E(n)$ exponentially large iteration times are needed, we construct $P_E(\ln n)$ instead (see also [20, 21]). Therefore, in Figs. 2(c,d) we present $P_E(\ln n)$ for the RL-fSM with $K = 6.908745$ and the same combinations of α and h used in panels (a,b) for $P_S(n)$.

To stress the fact that the panorama shown in Fig. 2 is generic for the RL-fSM, when the parameters K and α produce an ergodic phase space, in Fig. 3 we show $P_S(n)$ and $P_E(\ln n)$ now for $K = 7.5$ and several different combinations of α and h . In Fig. A.2 we present the Poincaré surfaces of section corresponding to the chosen values of α .

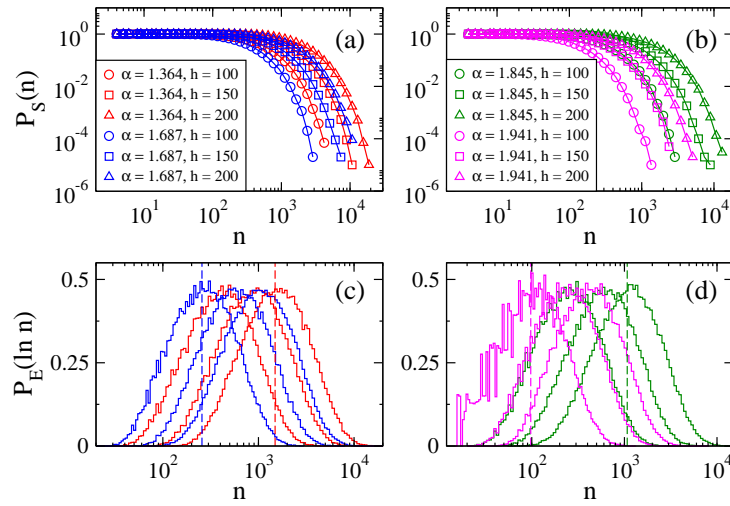


Figure 3: (a,b) Survival probability $P_S(n)$ as a function of n (symbols) for the RL-fSM with $K = 7.5$ and several combinations of α and h ($\alpha = 1.364$ in red, $\alpha = 1.687$ in blue, $\alpha = 1.845$ in green, and $\alpha = 1.941$ in magenta; h grows from left to right, as labeled in the figure). Full lines are fittings of the data with Eq. (6). Each curve was constructed by the use of $M = 10^5$ orbits. (c,d) Histograms for the frequency of escape $P_E(\ln n)$. Same color code as in (a,b). Vertical dashed lines are the typical escape times $n_{\text{typ}} = \exp\langle \ln n \rangle$ (they are shown for four histograms only to avoid figure saturation). Each histogram was constructed by the use of $M = 10^5$ orbits.

In [21] it was shown that the *typical iteration time*,

$$n_{\text{typ}} = \exp \langle \ln n \rangle, \quad (7)$$

characterizes well the maximum of $P_E(\ln n)$ of strongly chaotic systems. This fact is also valid for the RL-fSM with an ergodic phase space, as can be seen in Figs. 2(c,d) and Figs. 3(c,d) where n_{typ} is indicated with vertical dashed lines for selected histograms. Moreover, the relation between $P_E(n)$ and $P_S(n)$,

$$P_E(n) = -\frac{dP_S(n)}{dn}, \quad (8)$$

let us state that $\mu = n_{\text{typ}}$ and accordingly allow us to write

$$P_S(n) \approx \exp \left(-\frac{n}{n_{\text{typ}}} \right). \quad (9)$$

Note that in Eq. (9) we are writing approximately equal instead of equal. This is because we numerically found that $\mu \approx n_{\text{typ}}$, as can be seen in the insets of Figs. 4(a,b) where we plot n_{typ} vs. μ ; here μ is extracted from the fittings of Eq. (6) to the $P_S(n)$ curves of Figs. 2(a,b) and Figs. 3(a,b).

Expression (9) is of paramount importance because it reveals that $P_S(n)$ and accordingly $P_E(\ln n)$ depend on the ratio n/n_{typ} only; meaning that the typical iteration time [see Eq. (7)] is the scaling parameter of both quantities. In practical terms this means that when plotting $P_S(n)$ vs. n/n_{typ} and $P_E(\ln n)$ vs. n/n_{typ} , all curves will fall on top of universal curves independently of the parameter combination (K, α, h) . Indeed, we verify this last statement in Figs. 4(a,b) and Figs. 4(c,d) where we present $P_S(n)$ and $P_E(\ln n)$ as a function of n/n_{typ} , respectively, for the RL-fSM and several parameter combinations (in fact we are using the same curves reported in Figs. 2 and 3). As a reference we are also including Eq. (9) in Figs. 4(a,b) as black dashed lines to confirm that it describes relatively well the corresponding numerical data.

Finally, given the relevance of the typical iteration time for the scattering quantities we study here, it is mandatory to look for the dependence of n_{typ} on the system parameters (K, α, h) . Then, in Fig. 5(a) we plot n_{typ} as a function of K for several combinations of α and h and in Fig. 5(b) we report n_{typ} as a function of h for several combinations of α and K . Since from these figures we observe that n_{typ} depends on both K and h as power-laws, while

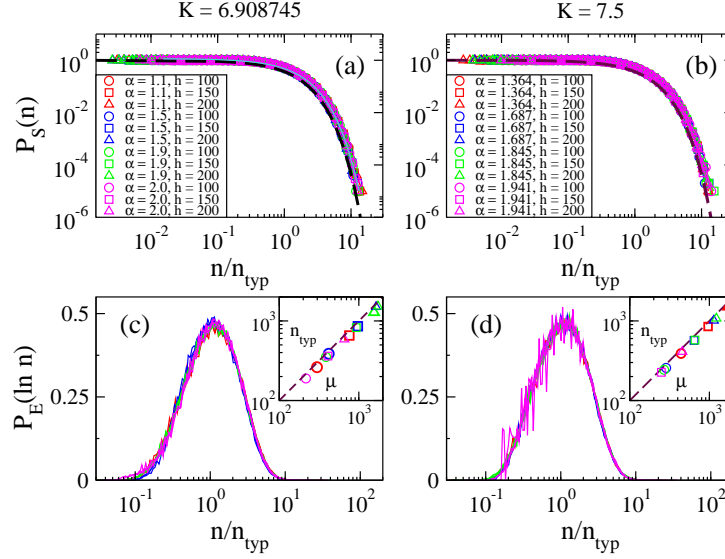


Figure 4: Survival probability $P_S(n)$ as a function of n/n_{typ} for the RL-fSM with (a) $K = 6.908745$ and (b) $K = 7.5$; same curves of (a) Figs. 2(a,b) and (b) Figs. 3(a,b). Dashed black lines in (a,b) correspond to Eq. (9). Insets in (c,d) show n_{typ} vs. μ . Here, μ is obtained from the fittings of the $P_S(n)$ curves of (a) Figs. 2(a,b) and (b) Figs. 3(a,b) with Eq. (6). The dashed lines corresponding to $n_{\text{typ}} = \mu$ are plotted to guide the eye.

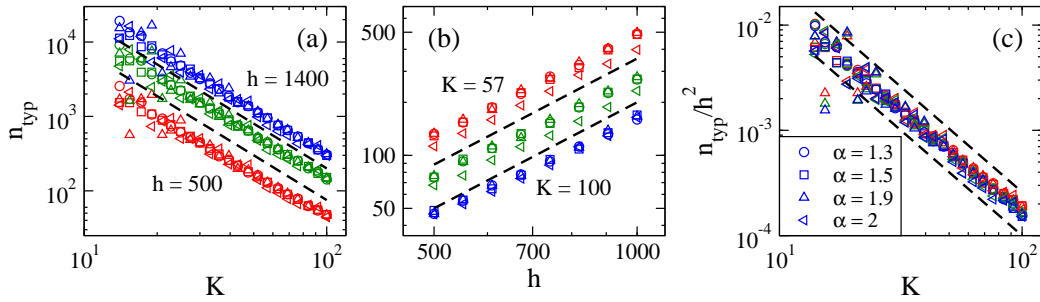


Figure 5: (a) Typical iteration time n_{typ} as a function of K for the RL-fSM. Here $h = 500$ (red symbols), $h = 950$ (green symbols), and $h = 1400$ (blue symbols); different values of α are shown: $\alpha = 1.3$ (\circ), $\alpha = 1.5$ (\square), $\alpha = 1.9$ (\triangle), and $\alpha = 2$ (\diamond). Black dashed lines proportional to K^{-2} are shown to guide the eye. (b) n_{typ} as a function of h . $K = 57$ (red symbols), $K = 76$ (green symbols), and $K = 100$ (blue symbols) for the values of α reported in (a). Black dashed lines proportional to h^2 are shown to guide the eye. (c) Typical escape time n_{typ} , normalized to h^2 , as a function of K . Same data as in panel (a). Black dashed lines proportional to K^{-2} are shown to guide the eye.

there is not an evident dependence on α , we propose the following scaling hypotheses for n_{typ} :

$$n_{\text{typ}} \propto K^{\gamma_K} h^{\gamma_h}. \quad (10)$$

where γ_K and γ_h are scaling exponents. By performing fittings of the data of Figs. 5(a,b) with Eq. (10) we obtained $\gamma_K \approx -2$ and $\gamma_h \approx 2$, see the dashed lines in Figs. 5(a,b). Indeed, by plotting now n_{typ}/h^2 vs. K , see Fig. 5(c), we better observe that $n_{\text{typ}} \propto K^{-2}$ and confirm the independence of n_{typ} on α . It is important to mention that (i) the values of γ_K and γ_h we found here for the RL-fSM were also reported for the discontinuous standard map in the quasilinear diffusion regime [21] and (ii) the behavior $n_{\text{typ}} \propto K^{-2}$ is clearly observed for relatively large values of K only, i.e. $K \gtrsim 30$; see Figs. 5(a,c).

3.2. Non-ergodic phase space

Once we verify that the escape of orbits from the phase space of the RL-fSM, when characterized by an ergodic phase space, is similar to that reported for strongly chaotic systems we compute the survival probability and the histograms for the frequency of escape when the phase space is non-ergodic. We again consider the RL-fSM with $K = 6.908745$ and $K = 7.5$, as in the previous subsection, but now we choose values of α which produce non-ergodic Poincaré surfaces of section, see Fig. A.3.

Then, in Figs. 6(a,b) we present $P_S(n)$ as a function of n for the RL-fSM with $K = 6.908745$ and two values of α [(a) $\alpha = 1.42$ and (b) $\alpha = 1.987$] for some values of h . In Figs. 6(c,d) we plot the corresponding $P_E(\ln n)$ histograms.

For increasing h both functions $P_S(n)$ and $P_E(\ln n)$ are displaced to the right as in the ergodic phase space case, see Figs. 2 and 3; this is expected since particles take longer to escape the higher the hole is. However, now $P_S(n)$ can not be described by a simple exponential decay, as in Eq. (6). We stress that not even the survival probability curves reported in Fig. 6(b), which look like simple exponentials, can be fitted by Eq. (6) in the complete range. This is not a big surprise since the exponential decay of $P_S(n)$ is only expected for strongly chaotic systems [18, 20, 21, 22], which is not the case with the values of α we chose in Fig. 6 [see Fig. A.3(a,b)]. Indeed, due to stickiness, $P_S(n)$ is known to develop asymptotic power-law tails in the case of mixed-chaotic dynamics [22, 23] and, due to Fermi acceleration, the decay of $P_S(n)$ as a stretched exponential was reported in [24].

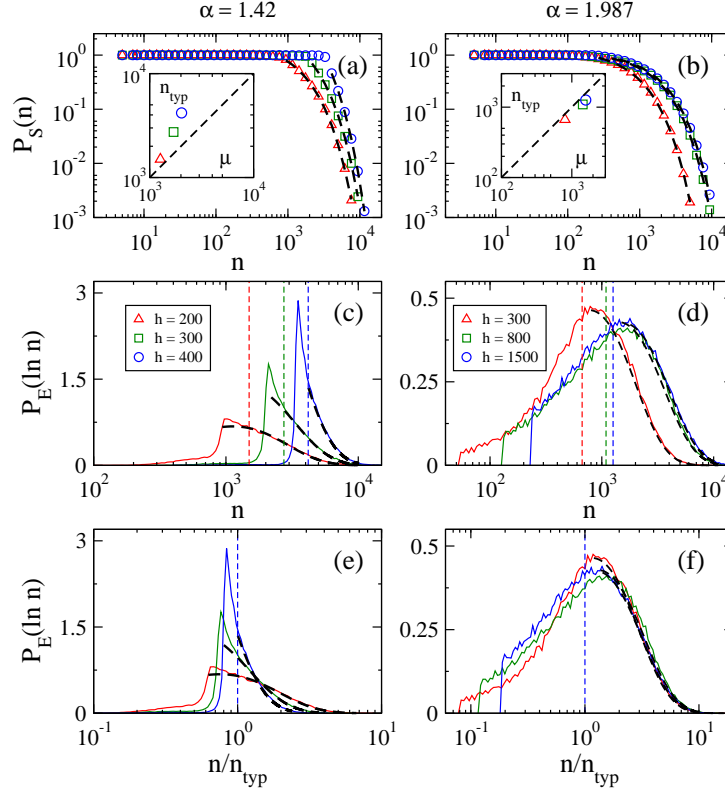


Figure 6: (a,b) Survival probability $P_S(n)$ as a function of n (symbols) for the RL-fSM with $K = 6.908745$ and several combinations of α and h : (a) $\alpha = 1.42$ and (b) $\alpha = 1.987$; h grows from left to right, as labeled in the figure. Dashed black lines are fittings of the data with Eq. (6). Each curve was constructed by the use of $M = 10^5$ orbits. Insets in (a,b) show n_{typ} vs. μ . Here, μ is obtained from the fittings of the $P_S(n)$ curves in the main panels with Eq. (6). The dashed lines corresponding to $n_{\text{typ}} = \mu$ are plotted to guide the eye. (c,d) Histograms for the frequency of escape $P_E(\ln n)$. Same color code as in (a,b). Vertical dashed lines are the typical escape times $n_{\text{typ}} = \exp\langle \ln n \rangle$. Each histogram was constructed by the use of $M = 10^5$ orbits. Black dashed lines are Eq. (11). (e,f) $P_E(\ln n)$ as a function of n/n_{typ} ; same histograms as in panels (c,d), respectively.

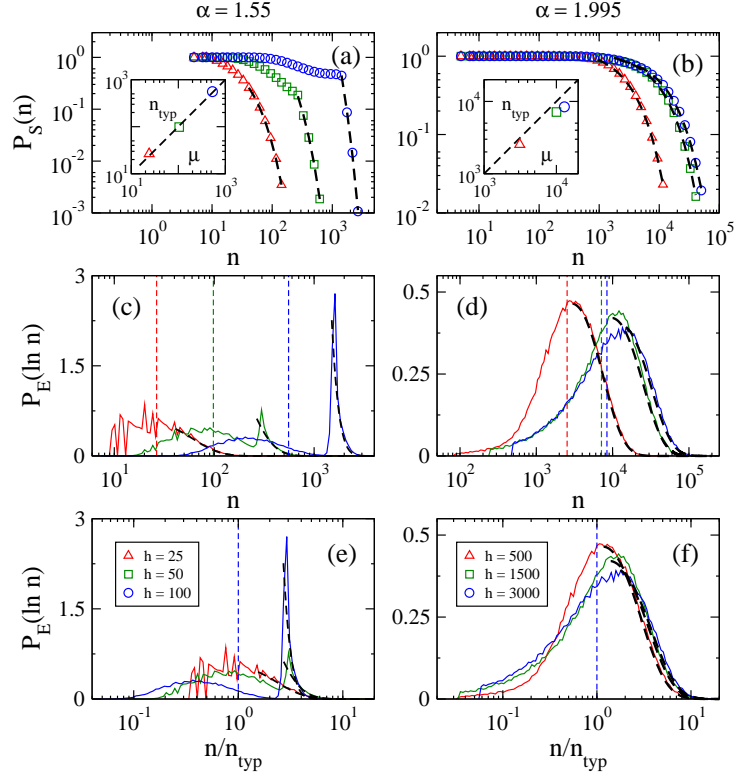


Figure 7: (a,b) Survival probability $P_S(n)$ as a function of n (symbols) for the RL-fSM with $K = 7.5$ and several combinations of α and h : (a) $\alpha = 1.55$ and (b) $\alpha = 1.995$; h grows from left to right, as labeled in the figure. Dashed black lines are fittings of the data with Eq. (6). Each curve was constructed by the use of $M = 10^5$ orbits. Insets in (a,b) show n_{typ} vs. μ . Here, μ is obtained from the fittings of the $P_S(n)$ curves in the main panels with Eq. (6). The dashed lines corresponding to $n_{\text{typ}} = \mu$ are plotted to guide the eye. (c,d) Histograms for the frequency of escape $P_E(\ln n)$. Same color code as in (a,b). Vertical dashed lines are the typical escape times $n_{\text{typ}} = \exp\langle \ln n \rangle$. Each histogram was constructed by the use of $M = 10^5$ orbits. Black dashed lines are Eq. (11). (e,f) $P_E(\ln n)$ as a function of n/n_{typ} ; same histograms as in panels (c,d), respectively.

In Fig. 7 we present $P_S(n)$ and $P_E(\ln n)$ for the RL-fSM now with $K = 7.5$ and (a,c) $\alpha = 1.55$ and (b,d) $\alpha = 1.995$. Here we also observe, as expected since the phase space is not ergodic [see Fig. A.3(c,d)], that $P_S(n)$ and $P_E(\ln n)$ strongly depend on the map parameters.

Nevertheless we found that the decay of $P_S(n)$ in both cases, Figs. 6(a,b) and 7(a,b), is indeed exponential for large times. See the black dashed lines in those panels which are fittings of the $P_S(n)$ curves with Eq. (6). Clearly, even when the tail of $P_S(n)$ can be fitted with Eq. (6), the values of μ extracted from the fittings can not always be identified with n_{typ} as displayed in the insets of Figs. 6(a,b) and 7(a,b). Luckily, once we know that the tail of $P_S(n)$ in Figs. 6(a,b) and 7(a,b) is well described by Eq. (6), by the use of Eq. (8) we can estimate the tail of $P_E(\ln n)$ as

$$P_E(\ln n) \sim \frac{n}{\mu} \exp\left(-\frac{n}{\mu}\right). \quad (11)$$

Indeed, Eq. (11) describes well the tail of $P_E(\ln n)$ for all the parameter combinations reported in Figs. 6(c,d) and 7(c,d), see the dashed lines.

Finally, it is pertinent to mention that even when we were able to describe the tails of $P_S(n)$ and $P_E(\ln n)$ with Eqs. (6) and (11), respectively, these scattering functions can not be scaled neither with n_{typ} nor with μ . See for example the histograms of $P_E(\ln n)$ as a function of n/n_{typ} in Figs. 6(e,f) and 7(e,f).

4. Discussion and conclusions

In this work we characterized the leaking of orbits from the phase space of the Riemann-Liouville fractional standard map (RL-fSM). The RL-fSM is parameterized by K and $\alpha \in (1, 2]$ which control the strength of nonlinearity and the fractional order of the derivative of the corresponding fractional kicked rotor. It is important to stress that, to the best of our knowledge, the scattering properties of maps with memory have not been explored before.

We computed the frequency of escape $P_E(n)$ and the survival probability $P_S(n)$, more specifically $P_S(\ln n)$, for a hole of height h placed in the action axis. We explored two scenarios: one where the phase space of the RL-fSM is ergodic, see e.g. Figs. A.1 and A.2, and another where the phase space is non-ergodic, see e.g. Fig. A.3.

When the phase space of the RL-fSM is ergodic we found that $P_E(n)$ and $P_S(\ln n)$ are both scale invariant with the typical escape time $n_{\text{typ}} =$

$\exp\langle \ln n \rangle$, so they are well described by universal curves; see Fig. 4. Moreover, for strongly chaotic systems, it has been shown that the survival probability can be obtained from the solution of the diffusion equation describing the transport of particles along the phase space as [19, 20]

$$P_S(n) \approx \exp\left(-\frac{\pi^2 D}{4h^2}n\right), \quad (12)$$

where D is the diffusion coefficient. Therefore, by equating Eqs. (9) and (12) and with the help of Eq. (10), we can infer the diffusion coefficient of the RL-fSM as

$$D \approx \frac{4}{\pi^2} \frac{h^2}{n_{\text{typ}}} \propto K^2. \quad (13)$$

It is relevant to highlight the independence of D on α .

When the phase space of the RL-fSM is not ergodic, even though we were able to characterize the tails of $P_E(n)$ and $P_S(\ln n)$ by means of Eqs. (6) and (11), respectively, both scattering functions showed clear non-universal and parameter-dependent behavior, see e.g. Figs. 6 and 7. That is, neither $P_E(n)$ nor $P_S(\ln n)$ can be scaled.

We hope that our results may motivate further numerical as well as theoretical studies on the scattering properties of fractional dynamical systems in the context of General Fractional Dynamics (GFDynamics), recently established by Tarasov in [17].

Appendix A.

To avoid the saturation of the main text, here we present the Poincaré surfaces of section for the RL-fSM with the parameters used to compute the survival probability $P_S(n)$ and the frequency of escape $P_E(\ln n)$ of Figs. 2-7.

Acknowledgements

J.A.M.-B. thanks support from CONACyT (Grant No. 286633), CONACyT-Fronteras (Grant No. 425854), VIEP-BUAP (Grant No. 100405811-VIEP2022), and Laboratorio Nacional de Supercómputo del Sureste de México (Grant No. 202201007C), Mexico. E.D.L. acknowledges support from CNPq (No. 301318/2019-0) and FAPESP (No. 2019/14038-6), Brazilian agencies.

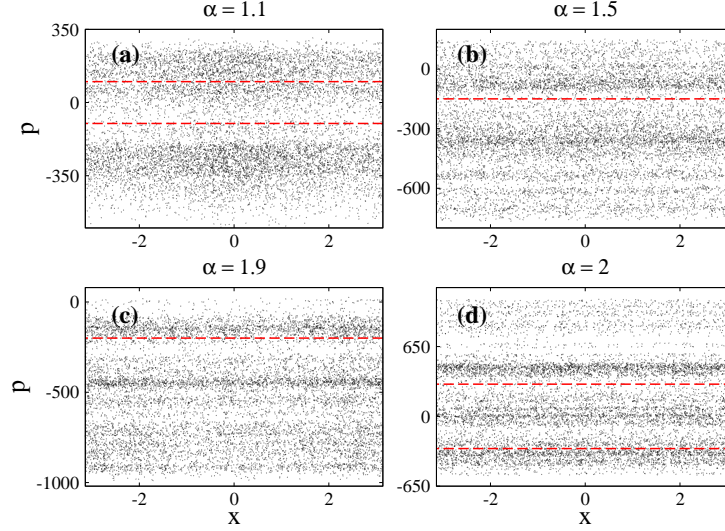


Figure A.1: Poincaré surfaces of section for the RL-fSM with $K = 6.908745$ for the values of α used to compute $P_S(n)$ and $P_E(\ln n)$ of Fig. 2. A single initial condition with $x_0 = 0$ and a random $p_0 \in (0, 2\pi/100)$ was iterated 10^4 times. Red dashed lines indicate the position of holes in the action axis at $p = \pm h$ with (a) $h = 100$, (b) $h = 150$, (c) $h = 200$, and (d) $h = 300$.

References

- [1] A. J. Lichtenberg, and M. A. Lieberman, *Regular and chaotic dynamics (Appl. Math. Sci.)* 38, Springer Verlag, New York (1992).
- [2] B. V. Chirikov, Research concerning the theory of nonlinear resonance and stochasticity, Preprint 267, Institute of Nuclear Physics, Novosibirsk (1969). Engl. Trans., CERN Trans. (1971) 71-40.
- [3] B. V. Chirikov, A universal instability of many-dimensional oscillator systems, *Phys. Rep.* **52** (1979) 263.
- [4] G. M. Zaslavsky, The simplest case of a strange attractor, *Phys. Lett. A* **69** (1978) 145–147.
- [5] F. Borgonovi, Localization in discontinuous quantum systems, *Phys. Rev. Lett.* **80** (1998) 4653.
- [6] M. Edelman and V. E. Tarasov, Fractional standard map, *Phys. Lett. A* **374** (2009) 279–285.

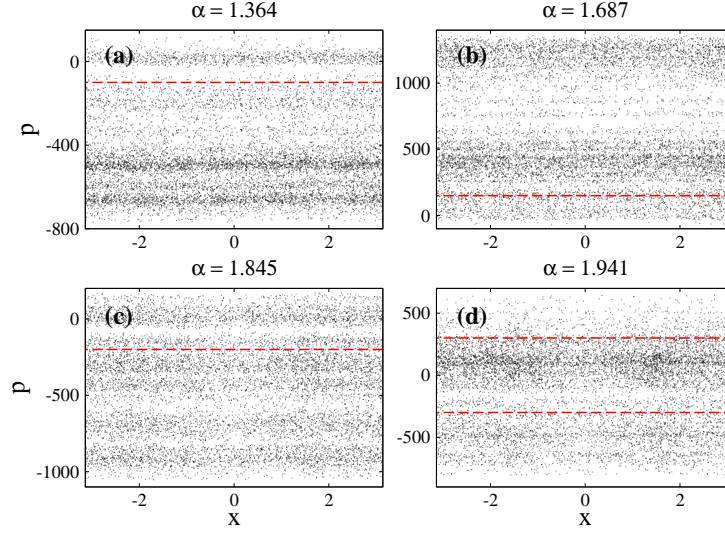


Figure A.2: Poincaré surfaces of section for the RL-fSM with $K = 7.5$ for the values of α used to compute $P_S(n)$ and $P_E(\ln n)$ of Fig. 3. A single initial condition with $x_0 = 0$ and a random $p_0 \in (0, 2\pi/100)$ was iterated 10^4 times. Red dashed lines indicate the position of holes in the action axis at $p = \pm h$ with (a) $h = 100$, (b) $h = 150$, (c) $h = 200$, and (d) $h = 300$.

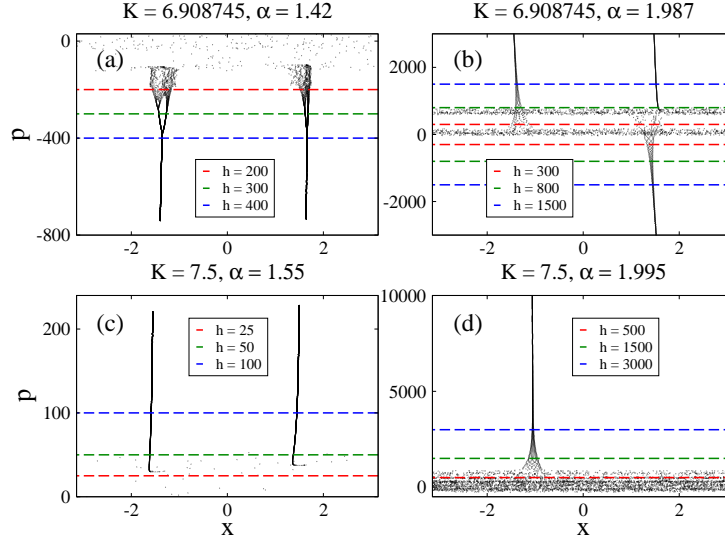


Figure A.3: Poincaré surfaces of section for the RL-fSM with (a,b) $K = 6.908745$ and (c,d) $K = 7.5$ for the values of α used to compute $P_S(n)$ and $P_E(\ln n)$ of Figs. 6 and 7. A single initial condition with $x_0 = 0$ and a random $p_0 \in (0, 2\pi/100)$ was iterated 10^4 times. Dashed lines indicate the position of holes in the action axis at $p = \pm h$.

- [7] V. E. Tarasov, *Fractional dynamics and discrete maps with memory*, in *Fractional Dynamics: Applications of Fractional Calculus To Dynamics Of Particles, Fields And Media*, Book Series in Nonlinear Physical Science, Springer, Berlin (2011) 409–453.
- [8] V. E. Tarasov, Integral equations of non-integer orders and discrete maps with memory, *Mathematics* **9** (2021) 1177.
- [9] V. E. Tarasov, Fractional dynamics with non-local scaling, *Commun. Nonlinear Sci. Numer. Simulat.* **102** (2021) 105947.
- [10] M. Edelman, Fractional standard map: Riemann-Liouville vs. Caputo, *Commun. Nonlinear. Sci. numer. Simulat.* **16** (2011) 4573–4580.
- [11] M. Edelman, Universal fractional map and cascade of bifurcations type attractors, *Chaos* **23** (2013) 033127.
- [12] V. E. Tarasov, and M. Edelman, Fractional dissipative standard map, *Chaos* **20** (2010) 023127.
- [13] V. E. Tarasov, *Fractional Zaslavsky and Henon discrete maps*, Chapter 1 in Long-range Interaction, Stochasticity and Fractional Dynamics, A. C. J. Luo and V. Afraimovich (Eds.), Springer, HEP (2010) 1–26.
- [14] V. E. Tarasov, Review of some promising fractional physical models, *Int. J. Modern Phys. B* **27** (2013) 1330005.
- [15] M. Edelman, Caputo standard α -family of maps: Fractional difference vs. fractional, *Chaos* **24** (2014) 023137.
- [16] G.-C. Wu, D. Baleanu, and S.-D. Zeng, Discrete chaos in fractional sine and standard maps, *Phys. Lett. A* **378** (2014) 484–487.
- [17] V. E. Tarasov, General fractional dynamics, *Mathematics* **9** (2021) 1464.
- [18] E. G. Altmann, J. S. E. Portela, and T. Tél, Leaking chaotic systems, *Rev. Mod. Phys.* **85** (2013) 869.
- [19] J. A. deOliveira, C. P. Dettmann, D. R. daCosta, and E. D. Leonel, Scaling invariance of the diffusion coefficient in a family of two-dimensional Hamiltonian mappings, *Phys. Rev. E* **87** (2013) 062904.

- [20] J. A. Méndez-Bermúdez, A. J. Martínez-Mendoza, A. L. P. Livorati, and E. D. Leonel, Leaking of trajectories from the phase space of discontinuous dynamics, *J. Phys. A: Math. Theor.* **48** (2015) 405101
- [21] J. A. de Oliveira, R. M. Perre, J. A. Méndez-Bermúdez, and E. D. Leonel, Leaking of orbits from the phase space of the dissipative discontinuous standard mapping, *Phys. Rev. E* **103** (2021) 012211.
- [22] T. Srokowski, J. Okolowicz, S. Drozd, and A. Budzanowski, Fusion cross section from chaotic scattering, *Phys. Rev. Lett.* **71** (1993) 2867.
- [23] A. L. P. Livorati, T. Kroetz, C. P. Dettmann, I. L. Caldas, and E. D. Leonel, Stickiness in a bouncer model: A slowing mechanism for Fermi acceleration, *Phys. Rev. E* **86** (2012) 036203.
- [24] C. P. Dettmann, and E. D. Leonel, Escape and transport for an open bouncer: Stretched exponential decays, *Physica D* **241** (2012) 403.